Probing the Magnetic Field of Light at Optical Frequencies

M. Burresi*[1], D. van Oosten[1], T. Kampfrath[1],
H. Schoenmaker[1], R. Heideman[2], A. Leinse[2], L. Kuipers[1]
[1]Center for Nanophotonics, FOM Institute AMOLF,
Science Park 113, 1098 XG Amsterdam, The Netherlands
[2]LioniX B.V., University of Twente
de Veldmaat 10, 7500 AH Enschede, The Netherlands

*burresi@amolf.nl.

Light is an electromagnetic wave composed of oscillating electric and magnetic fields, the one never occurring without the other. In light-matter interactions at optical frequencies the magnetic component of light generally plays a negligible role. When we "see" or detect light, only its electric field is perceived, we are practically blind to its magnetic component. We use concepts from the field of metamaterials to probe the magnetic field of light with an engineered near-field aperture probe. We visualize with sub-wavelength resolution the magnetic and electric field distribution of propagating light.

Text. As light interacts with matter, the force exerted by the electric field on a charge is c/v larger than the force applied by the magnetic field, where v is the velocity of the charge and c the speed of light. As a result, the response of a material to a magnetic field, e.g. the magnetic susceptibility, is a factor 10^{-4} smaller than the ease with which it is polarized, the dielectric susceptibility (***?***). Only when the charges move extremely fast, as for instance in relativistic

plasmas (*?, ?*), can the magnetic and electric coupling become comparable. In atomic systems, even though the magnetic dipole coupling is extremely weak, it is very important for fundamental tests of the standard model of particle physics (*?*). Magnetic light-matter interaction has been accomplished using artificial 'magnetic' atoms. By tailoring the geometry of such subwavelength metallo-dielectric structures effective magnetic coupling is achievable in the microwave regime (*?, ?*). Photonic nanostructures that resonantly respond to the magnetic field at optical frequencies can now be fabricated (*?, ?, ?, ?, ?*). This magnetic resonance can be exploited to study novel fascinating phenomena, such as negative index of refraction (*?*), super-lensing (*?*) and cloaking (*?, ?*). Whereas many advances have been made in controlling the light-matter coupling by magnetic means, the possibility of directly detecting the magnetic field at optical frequencies has not yet been explored. The ability to directly probe the magnetic field of light would of course be very beneficial to studies on metamaterials.

We use a near-field aperture probe, designed following split-ring resonator concepts, to detect the magnetic field at optical frequencies. Our probe is used to map the amplitude and phase of the magnetic field of propagating light. By also measuring the electric field, the magnetic and electric distributions of light can be mapped with subwavelength resolution.

We have fabricated a nanostructured metallo-dielectric probe to probe the magnetic field at optical frequencies. A sub-wavelength aperture has been created at the end of a tapered aluminum-coated single-mode fiber by focused ion beam milling (*?*). An air-gap of 40 nm is opened by focused ion beam milling in the coating. Such a split-probe is shown in the lower image of Fig. 1B. We compare the optical signals measured with a split-probe with those measured with a standard, cylindrically symmetric, coated probe (see upper image of Fig. 1B) that was used in the past (*?, ?, ?*). To ensure that we probe the magnetic field and rather than some signal caused by other electric field components, a well characterized single-mode Si_3N_4 ridge waveguide was used as a test structure (*?, ?*). Linearly polarized light from a laser diode

tuned to a wavelength of 1550 nm is coupled to the TE-mode of the waveguide. A fraction of the light in the waveguide is reflected by the end-facet, which sets up a standing wave inside the waveguide. This standing wave will cause a spatial amplitude modulation in both the electric and magnetic field components of the light. As in a standing wave the modulation of amplitude of the electric and magnetic components are shifted in space with respect to each other by half a period, this modulation is ideal to demonstrate that the magnetic field is being probed.

A phase-and polarization-sensitive near-field microscope is used for scanning and collecting the light (***?***), (Fig. 1A). The aperture of the probes couples the evanescent field of the light propagating through the waveguide to the probe-fiber (***?***). The light coupled into the probe-fiber is mixed with light in the reference branch of a Mach-Zehnder interferometer. Subsequently, the two orthogonal polarizations in the fiber are separated by a polarizing beamsplitter and simultaneously detected using a heterodyne scheme. By raster scanning the probe 20 nm above the sample, the amplitude and the phase distribution of the probed fields are obtained. The high symmetry of the standard probe was used to distinguish the two in-plane components of the electric field of propagating light (*?*). As a result of the symmetry of the aperture, the in-plane components of the electric field couple to the orthogonal modes of the probe fiber and are detected in the two separate channels of the microscope (Ch1 and Ch2). For an formal description of what the probe measures, we refer to the supporting online material (*?*). To probe the magnetic field of light, the magnetic field needs to be converted to an electric field before it can be measured at the detector. To achieve this conversion, the symmetry of the the conventional probe needs to be broken. This symmetry is broken in the split-ring probe used in this work, by introducing a single gap in the side of the metal coating. This is crucial, as a full ring or a ring with two opposing gaps would not exhibit the required optical bianisotropy (***?***, ***?***).

The waveguide is first characterized by performing near-field measurements with a standard probe (Fig 2A). The light propagates along $\hat{x}$, the electric field is along $\hat{y}$, the magnetic field

is along $\hat{z}$. Because the waveguide contains only a weakly guided TE-mode, the longitudinal component of the electric field is negligible (*?*, ***?***). The probe can be considered as a sub-wavelength metallic ring parallel to the sample surface, because of its cylindrical symmetry and the fact that the extension of the evanescent fields in air is only $\simeq 100$ nm (***?***). The evanescent electric field component E_y induces a dipolar charge distribution in the probe (see supporting online text). This induced oscillating dipole moment p_y couples to a propagating mode in the probe fiber and can be detected at the other end of the fiber. The magnetic field B_z, instead, generates a circular current in the ring, as described by Faraday's law. As a result, the probe exhibits a magnetic dipole moment m_z, in analogy with the magnetic response of a metallic cylinder (*?*). However, the radiation pattern of the magnetic dipole lies in the xy-plane and the cylindrical symmetry of the system forbids coupling of this magnetic dipole to the propagating modes in the probe fiber that propagate along $\hat{z}$. Therefore, the fields detected with a standard probe are the in-plane electric fields (*?*, ***?***).

Figure 2B shows the line-traces of the amplitude detected on Ch1 (red) and Ch2 (green), obtained by scanning the probe along the center of the waveguide. Because the only nonvanishing component of the electric field is along $\hat{y}$, we can attribute the signal detected by Ch1 to E_y and the Ch2-signal to E_x (Fig. 2A). Because in the center of the waveguide the longitudinal component (E_x) vanishes (*?*), Fig. 2B allows us to infer the experimental extinction ratio of the two polarization channels. As the ratio between the two amplitude signals is $\sim 1/20$ (in terms of intensity $\sim 1/400$), we are able to separate the two polarization states. As expected, an evident spatial amplitude modulation is present in both channels. Because the spatial period (~ 500 nm) is half a wavelength in the waveguide (*?*), this modulation is attributed to the standing wave caused by the interference between the forward propagating light and the small fraction of light that is reflected by the end-facet of the waveguide.

The sensitivity of the probe to the various field components of light changes drastically when

the split-probe is used. The air-gap is oriented along $\hat{y}$ (Fig. 2C). In analogy to the standard probe, E_y and B_z will induce in the split-probe an electric and magnetic dipole moment p_y and m_z, respectively. Like for the cylindrical probe, the dipole moment p_y will generate an optical signal in Ch1. However, due to the air-gap, the magnetically induced current cannot flow completely around the ring and will produce a time-varying dipolar charge distribution across the gap. This in-plane magnetically induced electric dipole moment can now couple to the fiber of the probe. Because the polarization of this radiation is along $\hat{x}$, the signal corresponding to B_z will be detected by Ch2. Hence, the optical signals with an electric and magnetic origin are detected in Ch1 and Ch2, respectively.

Figure 2D shows the measured amplitude of the Ch1- and Ch2-signal obtained with a split-probe. In contrast to Fig. 2B, the signals in the two channels have now comparable magnitude. The standing wave induced amplitude modulation of components of the two signals is roughly equal. However, the most important difference between Fig. 2B and 2D is that the maxima of the two standing waves are shifted in space by half a period. It is well known that in a standing light wave the amplitude of the magnetic field is shifted in space by half a period with respect to the amplitude of the electric field (***?***). The spatial shift of the local maxima that we observe in Fig. 2D is therefore a clear signature that Ch2 detects the light generated by the coupling with B_z. Thus, we have probed the out-of-plane component of the magnetic field.

To verify our claim of magnetic sensitivity of the probe, we perform an additional check. The same split-probe was used to measure on a waveguide oriented along $\hat{y}$, while keeping the air-gap oriented along $\hat{y}$ (Fig. 2E). In this configuration the electric field is along $\hat{x}$, rather than $\hat{y}$, and, thus, it should be detected by Ch2. However, B_z should also be detected by Ch2, because the orientation of the probe and, consequently, of the magnetically induced electric dipole moment has not changed. This means that the channel with higher signal should now be Ch2. This is indeed experimentally observed, as shown in Fig. 2F. Although the ratio between

the Ch1- and Ch2-signal is only $\simeq 0.27$ (in terms of intensity is $\simeq 0.07$), the ratio is higher than expected (see Fig. 2B). We attribute this to a minute in-plane rotation of the air-gap with respect to $\hat{y}$. When the air-gap is not perfectly aligned with $\hat{y}$, the probe projects a fraction of B_z on Ch1. More importantly, because in this configuration the split-probe does not separate E_x and B_z, the amplitude maxima of the two channels are no longer shifted in space with respect to each other, as indicated by the dashed lines in Fig. 2F.

In the above, we only considered the amplitude of the detected signals. To understand the mechanism of the split-ring probe, we have to analyze the phase difference $\Delta\phi$ between the complex signals in Ch1 and Ch2. As mentioned above, the magnetic field component of light induces a current in the ring, which in turn induces a time-varying charge distribution across the gap. Considering that we are far below the resonance freqyency of the split-probe (we estimate a resonant wavelength of $\lambda_o = 1300$ nm and a width $\Delta\lambda_o = 50$ nm for the resonance based on methods for split-ring resonators (*?*)), the current in de ring should be in phase with the driving magnetic field. The resulting electric dipole moment along $\hat{x}$ will oscillate 90 degrees out of phase with the current and, thus, 90 degrees out of phase with the driving magnetic field (see supporting online text). In short, the probe will respond to B_z with an electric dipole moment $p_x \propto \mathrm{i}B_z$, analogous to the magnetic response of split-ring resonators (***?***, *?*). Hence, From the curl equation $\nabla \times \mathbf{E} = -\partial\mathbf{B}/\partial t$, we know that for a plane wave traveling in the positive x direction, $\omega B_z = -kE_y$, where ω is the optical frequency and k the wave number of the light. Given the additional $\pi/2$ phase shift induced by the probe, the signal detected in Ch2 should be in quadrature with the E_y signal detected in Ch1. Figure 3A shows for different probes and setup conditions (such as the strain on the fiber and the orientation of the connectors) that we indeed consistently measure a constant phase difference $\Delta\phi = -\pi/2$ (with a spread of 10%) between Ch1 and Ch2, demonstrating that whereas Ch1 probes E_y, Ch2 shows $\mathrm{i}B_z$.

In Figs. 3B and C, the distributions of the raw data measured in Ch1 and Ch2 are shown,

collected by raster scanning the split-probe in the experimental configuration of Fig. 2C. As argued above, Ch1 and Ch2 correspond to the real part of E_y and $\mathbf{i}B_z$, respectively. The white dashed lines represent the position of the waveguide. A closer look at the wave fronts in Fig. 3B and C shows again that due to the detection mechanism of the probe, the two signals are shifted by $\pi/2$, where the green dashed lines can be used as guide to the eye (for further details see (*?*)). These images demonstrate that we simultaneously visualize with phase-sensitivity and sub-wavelength resolution the magnetic and electric field distribution of light propagating through a ridge waveguide. The simultaneous spatially resolved detection of both magnetic and electric fields should open up new fascinating research directions. By redesigning the geometry of the probe, it should be possible to detect other components of the light field, besides the three shown in this work. Furthermore, the split-probe can be used as a movable split-ring resonator and, thus, we can explore the local coupling between nano-objects that resonantly respond to the magnetic field at optical frequencies, such as split-ring resonators, double fishnet structures and stereometamaterials.

1. We gratefully thank M. Hammer and A. Ivanova for providing useful calculations and J.C. Prangsma and M. Spasenović for support and discussions. The authors gratefully acknowledge the support of the Smart Mix Programme of the Netherlands Ministry of Economic Affairs and the Netherlands Ministry of Education, Culture and Science. This work is part of the research program of the "Stichting voor Fundamenteel Onderzoek der Materie (FOM)", which is financially supported by the "Nederlandse organisatie voor Wetenschappelijk Onderzoek (NWO)". Support by the NWO (VICI grant) is gratefully acknowledged. This work is also supported by NanoNed, a nanotechnology program of the Dutch Ministry of Economic affairs. The authors declare to have no competing financial interests.

Fig. 1. (**A**) Schematic of the phase-sensitive near-field microscope. The near-field probe, indicated by the dashed box, is scanned 20 nm above the sample and collects through the aperture the evanescent field of the propagating light. Subsequently, the light is mixed with a reference branch of an interferometer. The resulting light is split by a polarizing beamsplitter and the two orthogonal polarizing components are detected with a heterodyne scheme. By suitably choosing the orientation of the two $\lambda/2$ waveplates, we can relate the signal at the two detectors, called Ch1 and Ch2, with the fields present in the sample. (**B**) A scanning electron micrograph of two aluminum coated near-field probes. For both probes the coating thickness is 150 nm and the aperture diameter is 200 to 230 nm. The upper image shows the highly cylindrical standard probe. The lower image shows a split-probe where an air-gap in the coating (indicated by the arrow) has been created.

Fig. 2. (**A**), (**C**) and (**E**) Schematic of the performed experiments. In the upper part, top views are shown. The 'ridge' has been colored differently for clarity. In the lower part, cross-sections in the zy-plane are shown. The red and green axes correspond to Ch1 and Ch2, respectively. (**A**), The standard probe is depicted in gray as a metallic ring. **C**, The split-probe is shown as a metallic split-ring. **E**, Same configuration than C but the waveguide is rotated by 90 degrees. (**B**), (**D**) and (**F**), Line-traces of the amplitude obtained scanning the probes along the waveguide. (**B**), Amplitude obtained with a standard probe (configuration shown in A). The line traces are normalized to the maximum of Ch1. Both signals show a standing wave component. (**D**), Amplitude obtained with a split-probe (configuration shown in C). The line traces are normalized to the maximum of Ch2. The Ch2-signal is comparable to Ch1. We associate the Ch2-signal with B_z. (**F**), Amplitude obtained with a split-probe (configuration shown in E). The line traces are normalized to the maximum of Ch2. Both E_x and B_z are projected along $\hat{x}$ and, thus, detected by Ch2.

Fig. 3. (**A**) Phase difference $\Delta\phi$ between the complex signals of Ch1 and Ch2 for the measurement of Fig. 3B for different experimental conditions. (**B**) and (**C**). Normalized Distributions of Re(E_y) and Re(iB_z), respectively. The images have been obtained by raster scanning the split-probe in the configuration shown in Fig. 2C over an area 2.2×3.4 μm^2. The white dashed lines represent the position of the waveguide. The green dashed line is a guide to the eye that indicates the $\pi/2$ phase shift of the two wave fronts.

FIGURE 1

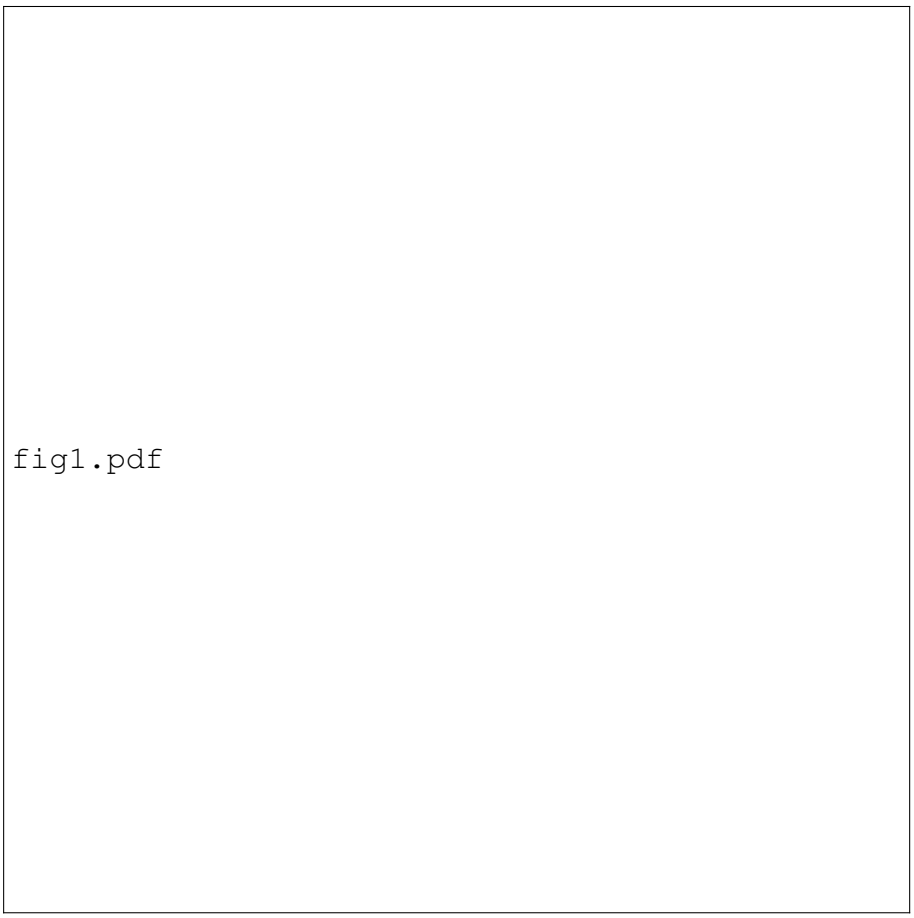

FIGURE 2

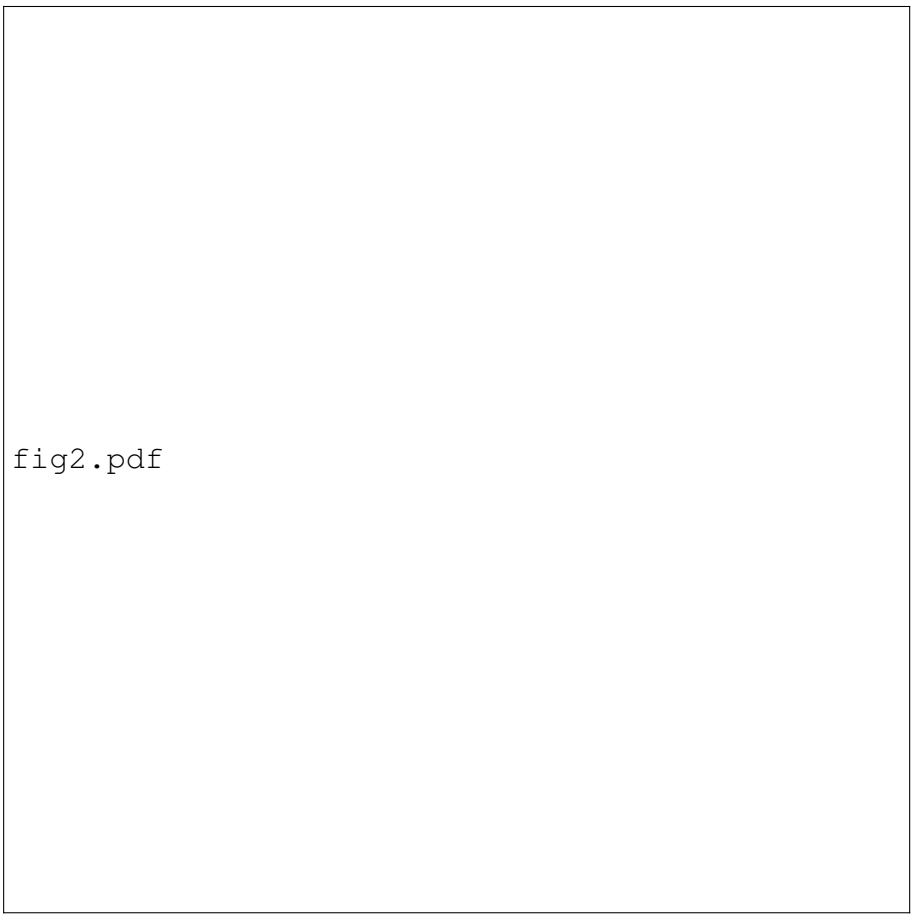

FIGURE 3

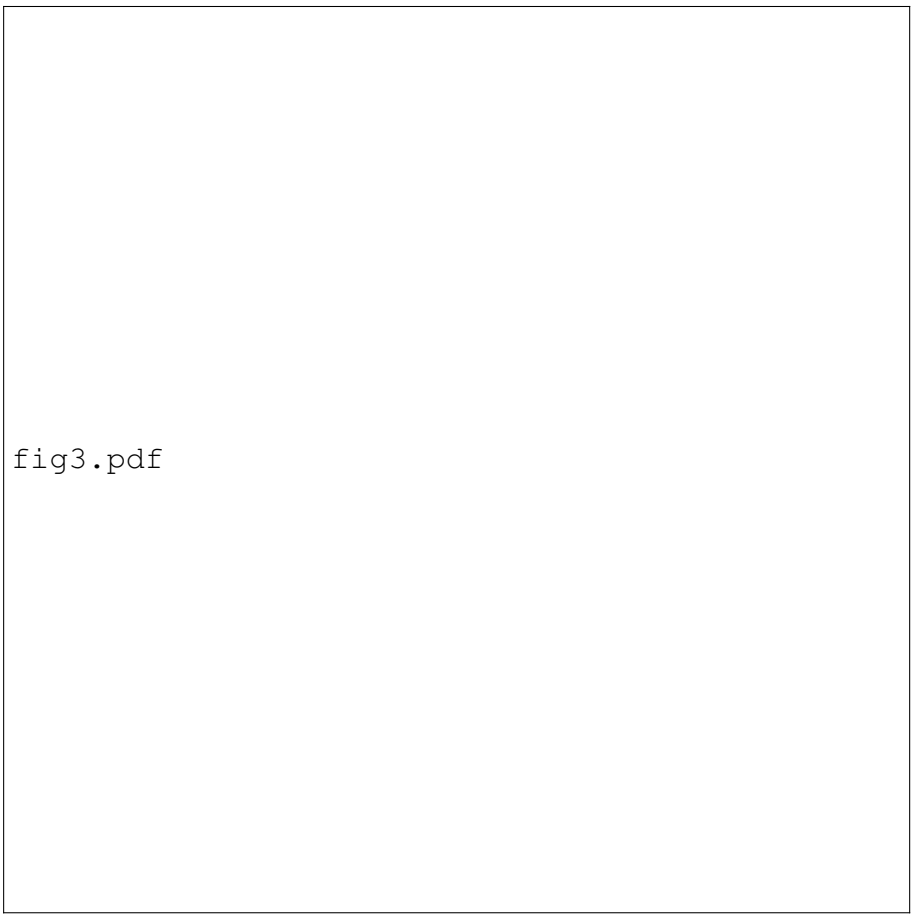

Supporting Online Material for Probing the Magnetic Field of Light at Optical Frequencies.

M. Burresi*, D. van Oosten, T. Kampfrath,

H. Schoenmaker, R. Heideman, A. Leinse, L. Kuipers

*burresi@amolf.nl.

Supporting Online Material

Materials and methods. We investigate the optical properties of the split-probe on two types of ridge waveguide. For both the waveguides we started with a Si wafer of 525 μm thick on top of which an 8 μm layer of thermal silicon oxide has been grown. The first waveguide has been obtained by growing a 170 nm Si_3N_4 layer and subsequently by dry etching a straight ridge with a width of 2 μm and a height of 20 nm. The waveguide supports only a weakly guided TE mode. The waveguide has an effective refractive index of ~ 1.46 and for an incident wavelength of 1550 nm the wavelength in the structure is $\lambda \sim 1550/1.46$ nm $\simeq 1060$ nm. In such a waveguide the longitudinal component E_x of the electric field is maximally 10% of the transverse component E_y. E_x has an antisymmetric distribution with respect to the waveguide and its maximum amplitude is located close to the edge of the ridge. We attribute the slight asymmetry of Fig. 3C to the antisymmetric contribution of E_y to the B_z-signal detected on Ch2. In order to measure with a rotated probe-ridge orientation, we use another waveguide with two straight sections connected by a 90 degrees bend. To guide the light across the bend a stronger effective refractive index contrast is required. This is achieved using a 300 nm thick Si_3N_4 layer. This waveguide turns out to be single-mode for TE and TM. The waveguide has an effective refractive index of ~ 1.6 and, thus, the wavelength in the structure is $\lambda \sim 1550/1.6$ nm $\simeq 970$ nm.

Supporting online text. Polarizabilities of standard probes. We consider a standard probe as a metallic ring. Due to the symmetry of the ring, the in-plane electric polarizabilities $\alpha_{xx}^{\mathrm{ee}} = \alpha_{yy}^{\mathrm{ee}} \neq 0$. Because in the investigated waveguide the vertical component of the electric field is negligible, we do not consider the out-of-plane polarizability $\alpha_{zz}^{\mathrm{ee}}$. The linear response of the probe to an in-plane electric field is an induced in-plane electric dipole moment $p_j = \alpha_{jj}^{\mathrm{ee}} E_j$, where the label j is either $\hat{x}$ or $\hat{y}$.

The only nonvanishing magnetic polarizability of the standard probe is $\alpha_{zz}^{\mathrm{mm}}$, which can be estimated by Faraday's law. The probe responds to an out-of-plane magnetic field with an induced out-of-plane magnetic dipole moment $m_z = \alpha_{zz}^{\mathrm{mm}} B_z$. Due to the small penetration of the in-plane magnetic field into the metallic ring, the in-plane magnetic polarizabilities can be considered negligible.

Polarizabilities of split-probes. We describe the split-probe as a metallic split-ring. The considerations for the standard probe also apply here for the polarizabilities $\alpha_{xx}^{\mathrm{ee}}$, $\alpha_{yy}^{\mathrm{ee}}$, $\alpha_{zz}^{\mathrm{ee}}$ and $\alpha_{zz}^{\mathrm{mm}}$, with the exception that $\alpha_{xx}^{\mathrm{ee}} \neq \alpha_{yy}^{\mathrm{ee}}$. Moreover, due to the air-gap in the probe, B_z induces an in-plane electric dipole moment $p_x = \mathbf{i}\alpha_{xz}^{\mathrm{em}} B_z$. Likewise, E_x induces a vertical magnetic dipole moment $m_z = \mathbf{i}\alpha_{zx}^{\mathrm{me}} E_x = -\mathbf{i}\alpha_{xz}^{\mathrm{em}} E_x$.